PNAS Nexus, 2024, 3, 1–12
https://doi.org/10.1093/pnasnexus/pgae002
Advance access publication 4 January 2024
Research Report

G-protein signaling of oxytocin receptor as a potential target for cabazitaxel-resistant prostate cancer

Hiroshi Hongo[a], Takeo Kosaka[a,*], Ken-Ichi Takayama[b], Yuto Baba[a], Yota Yasumizu[a], Koji Ueda[c], Yutaka Suzuki[d], Satoshi Inoue[b,e], Himisha Beltran[f,g] and Mototsugu Oya[a]

[a]Department of Urology, Keio University School of Medicine, Shinjuku-ku, Tokyo 160-8582, Japan
[b]Department of Systems Aging Science and Medicine, Tokyo Metropolitan Institute of Gerontology, Itabashi-ku, Tokyo 173-001, Japan
[c]Cancer Proteomics Group, Cancer Precision Medicine Center, Japanese Foundation for Cancer Research, Koto-ku, Tokyo 135-8550, Japan
[d]Department of Computational Biology and Medical Sciences, Graduate School of Frontier Sciences, The University of Tokyo, Chiba 277-8562, Japan
[e]Division of Systems Medicine and Gene Therapy, Saitama Medical University, Hidaka, Saitama 350-1298, Japan
[f]Department of Medical Oncology, Dana Farber Cancer Institute, Boston, MA 02215, USA
[g]Department of Medicine, Harvard Medical School, Boston, MA 02215, USA
*To whom correspondence should be addressed: Email: takemduro@gmail.com
Edited By: JoAnn Trejo

Abstract

Although the treatment armamentarium for patients with metastatic prostate cancer has improved recently, treatment options after progression on cabazitaxel (CBZ) are limited. To identify the mechanisms underlying CBZ resistance and therapeutic targets, we performed single-cell RNA sequencing of circulating tumor cells (CTCs) from patients with CBZ-resistant prostate cancer. Cells were clustered based on gene expression profiles. In silico screening was used to nominate candidate drugs for overcoming CBZ resistance in castration-resistant prostate cancer. CTCs were divided into three to four clusters, reflecting intrapatient tumor heterogeneity in refractory prostate cancer. Pathway analysis revealed that clusters in two cases showed up-regulation of the oxytocin (OXT) receptor–signaling pathway. Spatial gene expression analysis of CBZ-resistant prostate cancer tissues confirmed the heterogeneous expression of OXT-signaling molecules. Cloperastine (CLO) had significant antitumor activity against CBZ-resistant prostate cancer cells. Mass spectrometric phosphoproteome analysis revealed the suppression of OXT signaling specific to CBZ-resistant models. These results support the potential of CLO as a candidate drug for overcoming CBZ-resistant prostate cancer via the inhibition of OXT signaling.

Keywords: oxytocin, cabazitaxel-resistant prostate cancer, G-protein signaling

Significance Statement

Although the treatment armamentarium for patients with metastatic prostate cancer has improved recently, treatment options after progression on cabazitaxel (CBZ) are limited. We performed single-cell RNA sequencing of circulating tumor cells (CTCs) from patients with CBZ-resistant prostate cancer. In silico screening was used to nominate candidate drugs for overcoming CBZ resistance in castration-resistant prostate cancer. CTCs were divided into three to four clusters, reflecting intrapatient tumor heterogeneity in refractory prostate cancer. Pathway analysis revealed that clusters in two cases showed up-regulation of the oxytocin (OXT) receptor–signaling pathway. Cloperastine (CLO) had significant antitumor activity against CBZ-resistant prostate cancer cells. Phosphoproteome analysis revealed the suppression of OXT signaling specific to CBZ-resistant models.

Introduction

Prostate cancer is the most common cancer among men and the second most common cause of cancer-related deaths worldwide (1). Metastatic prostate cancer is mainly treated using gonadotropin-releasing hormone agonists/antagonists and nonsteroidal antiandrogens. Although androgen deprivation therapy is initially effective for prostate cancer, most patients develop castration-resistant prostate cancer (CRPC). Taxanes, such as docetaxel (DOC) and cabazitaxel (CBZ), are the only chemotherapy regimens approved for CRPC. CBZ, a next-generation taxane, was approved in 2010 for DOC-resistant prostate cancer. However, its life-prolonging effect in CRPC is limited to a few months (2), and CBZ-resistant prostate cancer has an extremely poor prognosis of <1 year (2, 3). Therefore, there is an urgent need to develop novel therapeutic strategies for CBZ-resistant prostate cancer.

We have previously reported the feasibility and value of genomic analysis of prostate cancer tissues for precision medicine (4–6). As biopsy of refractory tissue is often impractical, liquid biopsy, including that of cell-free DNA and circulating tumor cells (CTCs), may be an alternative for molecular characterization of

Competing Interest: The authors declare no competing interest.
Received: July 10, 2023. **Accepted:** December 27, 2023
© The Author(s) 2024. Published by Oxford University Press on behalf of National Academy of Sciences. This is an Open Access article distributed under the terms of the Creative Commons Attribution-NonCommercial-NoDerivs licence (https://creativecommons.org/licenses/by-nc-nd/4.0/), which permits non-commercial reproduction and distribution of the work, in any medium, provided the original work is not altered or transformed in any way, and that the work is properly cited. For commercial re-use, please contact journals.permissions@oup.com

treatment-resistant prostate cancer (7). Prostate cancer has a high degree of tumor heterogeneity. Therefore, a liquid biopsy-based analysis could better capture its heterogeneity within and across metastases in individuals with CRPC (8). Recent studies have performed single-cell RNA sequencing (RNA-seq) of CTCs in the liver (9), breast (10), and lung cancers (11).

Although the efficacy of single-cell transcriptomic analysis of CTCs in prostate cancer has been reported (12), single-cell transcriptomes of CBZ-resistant prostate cancer have not yet been studied. Therefore, to screen for therapeutic targets, this study performed a single-cell transcriptomic analysis of CTCs of patients with CBZ-resistant prostate cancer, collected in a label-free state through our established platform (7). Furthermore, we performed spatial transcriptomic analysis of CBZ-resistant prostate cancer tumor tissues to analyze intratumoral heterogeneity and validate the significance of molecular markers identified via single-cell RNA-seq of CTCs.

We have previously established CBZ-resistant prostate cancer cell lines (13). Instead of screening for signaling pathways or gene products with potential therapeutic targets from the lists of CBZ-resistance-associated genes, we submitted the gene lists directly to the Connectivity Map database (14). This public resource contains gene signatures obtained after treating the cells with various chemical compounds. Using this drug-screening platform, we identified ribavirin (15, 16), pimozide (17), and etoposide (18) as novel drugs for overcoming taxane-resistant prostate cancer.

Using our established approach, this study is the first to report single-cell transcriptomic and spatial gene expression analyses of CBZ-resistant prostate cancer. We identified oxytocin (OXT) signaling as a potential therapeutic target. Furthermore, we performed an in silico screening test for candidate drugs targeting CBZ resistance, analyzed target signals of candidate drugs by a phosphoproteome analysis using liquid chromatography–mass spectrometry (LC–MS), and identified cloperastine (CLO) as a candidate drug to suppress OXT signaling in CBZ-resistant prostate cancer.

Results

OXT signaling is up-regulated in CBZ-resistant prostate cancer

CTCs were collected and concentrated from four patients with prostate cancer after CBZ resistance. The patients' clinical characteristics are shown in Table S1. We performed single-cell RNA-seq on CTCs using the 10× Genomics Chromium system, and the cells were clustered based on their gene expression profiles. The CTCs of each patient were divided into three or four clusters based on their expression (Figs. 1A and B and S1 and S2), reflecting intrapatient tumor heterogeneity in refractory prostate cancer.

To screen for potential therapeutic targets for CBZ-resistant prostate cancer, we performed pathway analysis using the database for annotation, visualization, and integrated discovery (DAVID) functional annotation clustering tool. We listed the significantly up-regulated gene expressions (over two times above average) in each cluster derived from single-cell RNA-seq. Pathway analysis revealed that the OXT-signaling pathway (KEGG PATHWAY ID: hsa04921) was significantly enriched in cluster 3 of KOU805 ($P = 0.038$) and cluster 1 of KOU809 ($P = 0.035$) compared to the other clusters (Figs. 1C and S3). Oxytocin receptor (OXTR) and downstream signaling molecules, such as G-protein subunit alpha q (GNAQ), calmodulin (CALM) 2, protein kinase C beta (PRKCB), myosin light polypeptide (MYL) 6, and fos proto-oncogene (FOS), were enhanced in the clusters with up-regulated OXT signaling pathway (Fig. 1D and E). The expression level of other OXT signal-related molecules was also relatively high in cluster 3 of KOU805 and cluster 1 of KOU809 (Fig. S4).

CD46 has been reported as a poor prognostic marker in prostate cancer (19, 20). We found that the two clusters were characterized by CD46, which was also up-regulated in cluster 3 of KOU805 and cluster 1 of KOU809, along with OXT signaling pathways (Fig. S7), indicating the important role of these clusters in disease progression. Downstream molecules of OXT signaling, such as myosin light chain kinase, MYL6, and FOS, were expressed in cluster 3 of KOU801 and cluster 4 of KOU803, although only slight OXTR expression was observed in these clusters (Fig. S5).

To investigate the clinical significance of OXT signaling molecules in CBZ-resistant prostate cancer, we compared their mRNA expression before and after CBZ chemotherapy in five patients (Table S2) using microarray. Although OXT and OXTR expression levels were not significantly different before and after chemotherapy, that of phosphoinositide phospholipase C beta (PLCB) 3, a downstream molecule of OXT signaling was significantly up-regulated ($P = 0.023$) after CBZ (Fig. S6).

To investigate the significance of OXT signaling in CBZ-resistant prostate cancer, phosphoproteome analysis using LC–MS was performed to comprehensively explore the changes in signaling pathways induced by CBZ resistance. Pathway analysis revealed enhanced phosphorylation of OXT signaling proteins in DU145CR (DU145 CBZ-resistant) cells compared with that in parental DU145 cells (Fig. 1F and H). The phosphorylation of OXT-signaling-related molecules, such as calcium/CALM-dependent protein kinase (CAMK) 2D/G, EEE2K, GNAI2, MAPK1, PLCB3, PRKAA1, and rho-associated protein kinase (ROCK) 2, was higher in DU145CR cells than in DU145 cells (Fig. 1G).

Analysis of a previously reported NGS (next-generation sequencing) study of cancer cell lines (21) revealed that OXTR expression was higher in CRPC cell lines, DU145 and PC3, than in the hormone-naive prostate cancer cell lines, such as LNCAP, MDAPCA2B, and PRECLH, whereas all prostate cancer cell lines, including DU145 and PC3, had a low mRNA expression of OXT (Fig. S8). OXT signaling molecules, such as GNAQ and CALM2, were expressed in DU145 cells (Fig. S8). We also analyzed the mRNA expression of OXT and OXTR in CBZ-resistant cell lines and found no differences in the expression of these genes between CBZ-sensitive and CBZ-resistant cell lines (Fig. S9). According to these findings, proteins involved in OXT signaling were expressed to some extent in the CBZ-naïve parental cell lines. Although their expression was not changed, the phosphorylation of OXT signaling molecules was enhanced in CBZ-resistant cell lines.

To investigate intratumor heterogeneity of OXT signaling in CRPC, we performed spatial gene expression analysis of prostatic carcinoma specimens obtained by transurethral resection from two patients with prostate cancer who were heavily treated and developed resistance to CBZ therapy (Table S3). RNA expression in the tumor tissues was divided into six or seven clusters, suggesting intratumoral heterogeneity (Figs. 2A and B and S10A and B). The prostate specimens showed heterogeneous expression of OXT-signaling molecules, such as OXTR. In addition, PLCB3 and EEF2K were up-regulated in cluster 5 of KT304 and cluster 2 of KOV002 (Fig. 2C–E).

CLO is a candidate drug for overcoming CBZ-resistant prostate cancer

We analyzed the transcriptomic changes after CBZ resistance by comparing DU145 and PC3 cells with CBZ-resistant DU145CR and PC3CR (PC3 CBZ-resistant) cells. Based on the transcriptome

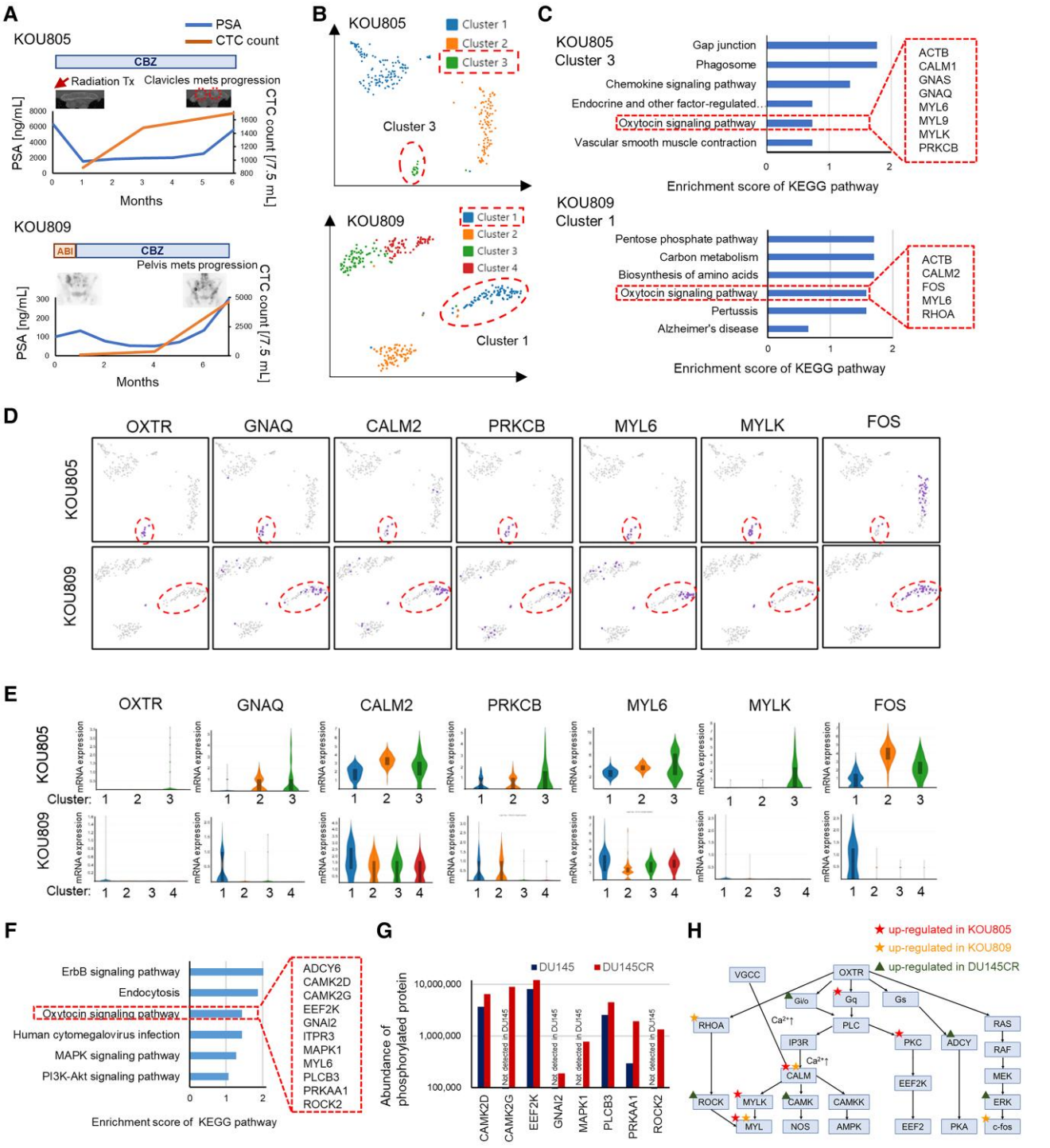

Fig. 1. OXT signaling is up-regulated in CBZ-resistant prostate cancer. A) Clinical course of the two cases. B) T-distributed stochastic neighbor embedding (t-SNE) plot based on the single-cell transcriptome in two patients with prostate cancer. Dotted circles and squares indicate the clusters with up-regulated OXT signaling. C) Pathway analysis showed that the two cases had clusters with an up-regulated OXT-signaling pathway. The dotted squares indicate up-regulated genes related to OXT signaling in each case. D) Expression of OXT, OXTR, GNAQ, CALM2, PRKCB, and MYL6. Intense purple dot plots indicate the cells with significantly higher expression of each gene. Dotted circles indicate the clusters with up-regulated OXT signaling. E) Violin plot of OXT, OXTR, GNAQ, CALM2, PRKCB, and MYL6. F) Pathway analysis of highly phosphorylated molecules in DU145CR compared to DU145. The dotted squares indicate up-regulated genes related to OXT signaling in DU145CR. G) Phosphorylation of each molecule of the OXT-signaling pathway in DU145 and DU145CR cells. H) Scheme of OXT-signaling pathway.

data, we performed in silico drug screening for candidate drugs that reverted the CBZ-resistant gene signature into a CBZ-sensitive signature (Fig. 3A and Table S4). We tested the anti-tumor effects of the listed candidate drugs on prostate cancer cell lines in vitro. Lanatoside C, practolol, meteneprost, and sanguinarine did not significantly inhibit DU145CR proliferation (Fig. S11), whereas CLO significantly suppressed DU145CR cell proliferation, not that of DU145 (Fig. 3B).

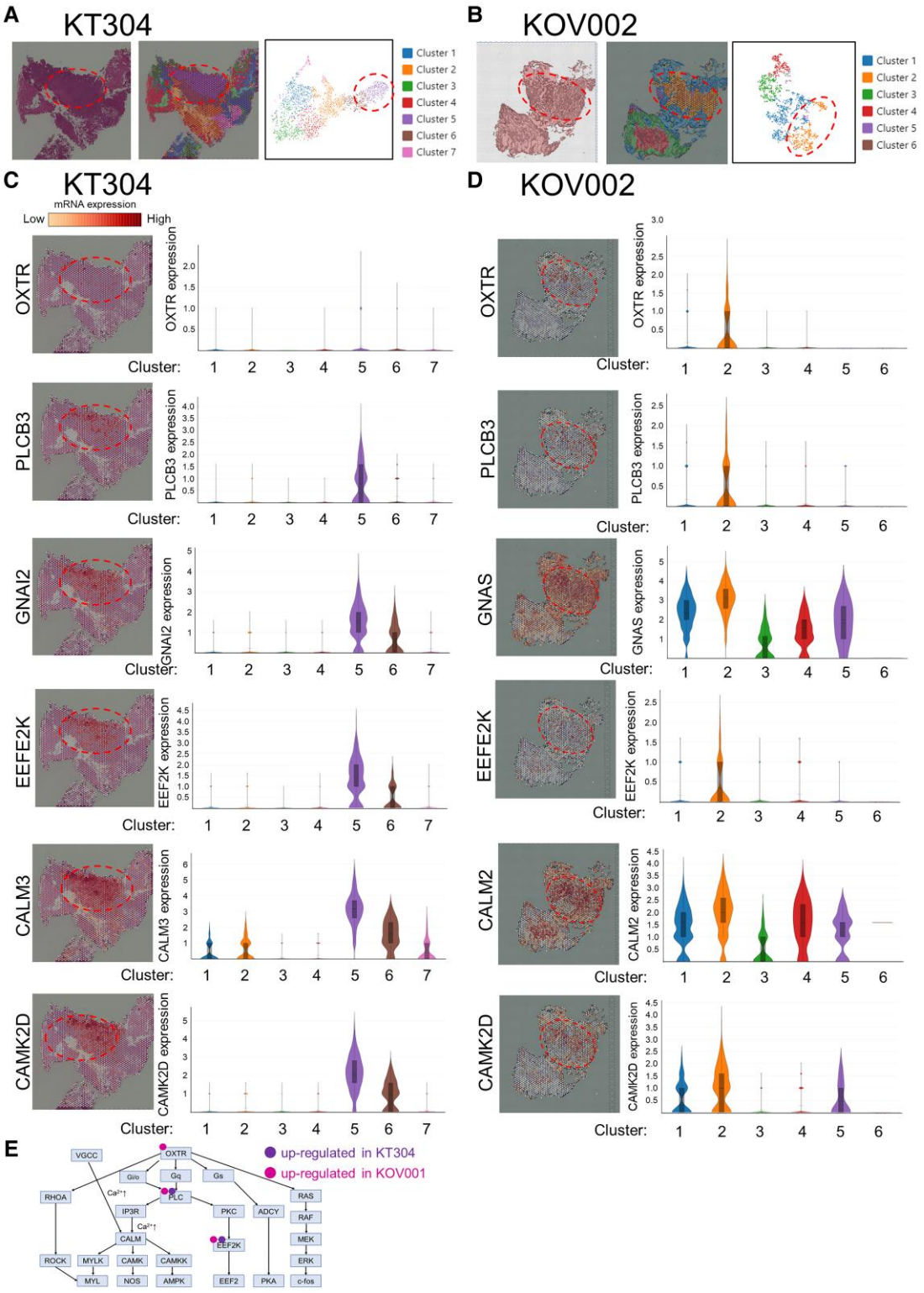

Fig. 2. Spatial gene expression analysis of CBZ-resistant prostate cancer tissues. A and B) Hematoxylin and eosin staining (left), spatial gene expression clustering (middle), and t-SNE plot according to gene expression (right) of prostatic tissue in KT304 (A) and KOV002 (B). The dotted square indicates a gene related to OXT signaling. C) Spatial mRNA expression (left) and violin plot (right) of OXTR, PLCB3, GNAI2, EEF2K, CALM3, and CAM2KD in KT304. D) Spatial mRNA expression (left) and violin plot (right) of OXTR, PLCB3, G-protein subunit alpha s (GNAS), EEF2K, CALM2, and CAM2KD in KT304. E) Scheme of OXT-signaling pathway.

We subsequently tested the synergistic effects of CBZ and CLO in DU145CR cells. The combination index of CBZ and CLO was 0.76, suggesting that they exhibited antitumor synergy (Fig. 3C). CLO also suppressed PC3CR cell proliferation in vitro (Fig. S12A and B).

We administered CLO to DU145 and DU145CR xenograft mouse models to investigate the antitumor effect of CLO in vivo. Daily peroral administration of CLO exerted antitumor effects in both DU145 and DU145CR xenograft tumors (Fig. 3D and E), and the growth of DU145CR tumors was suppressed to a greater extent

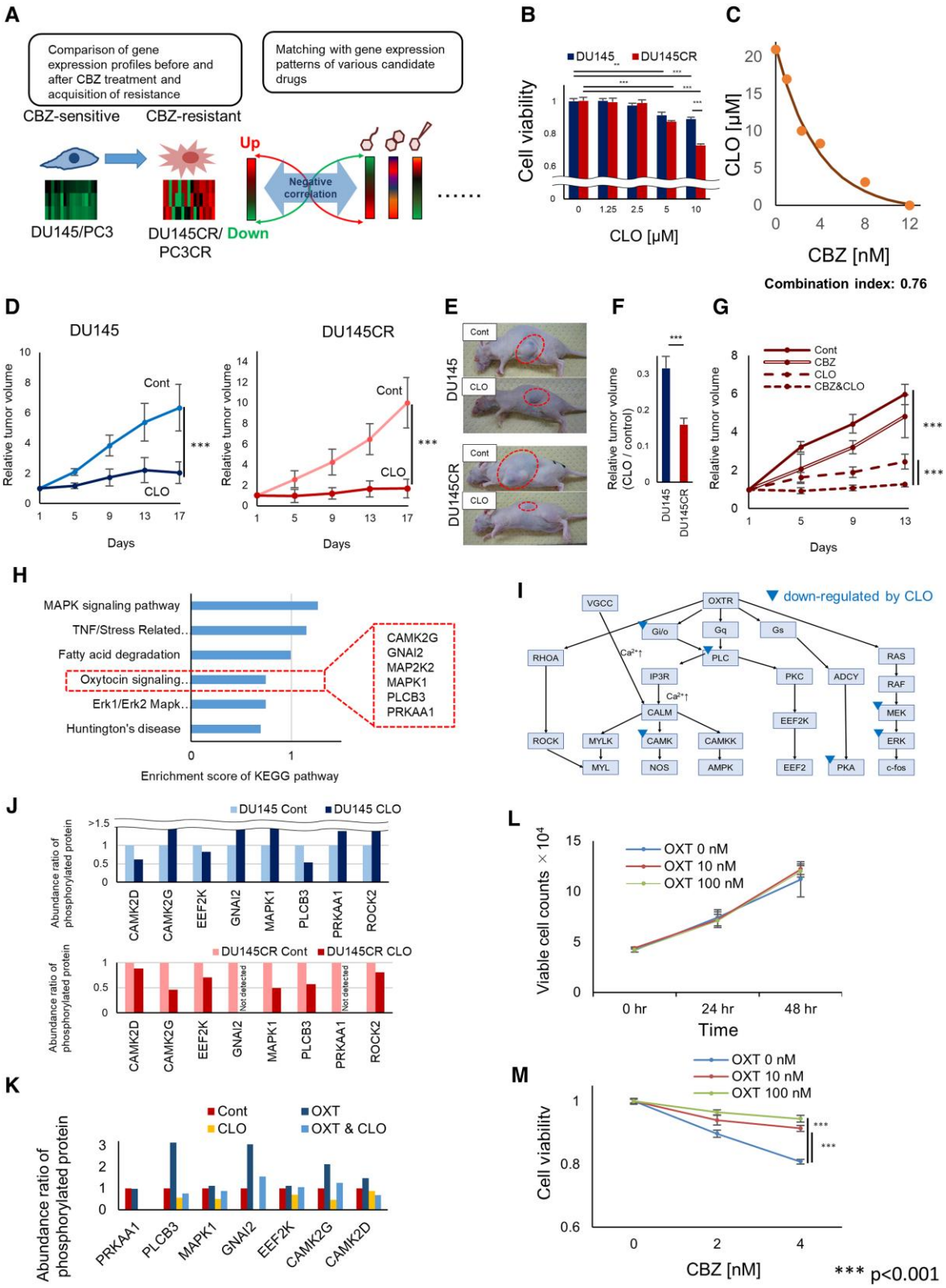

Fig. 3. CLO is an effective drug for taxane resistance. A) Schema of in silico screening for overcoming taxane-resistant prostate cancer. B) Viability of DU145 and DU145CR cells treated with various doses of CLO. C) Isobologram plots of the interactions between CLO and CBZ. Each dot on the plot represents the concentration of CLO and CBZ required to achieve IC50. E) Photographs of xenograft mice on day 17. F) Relative tumor volume of CLO groups compared to control groups in DU145/DU145CR xenograft models. G) Tumor growth over time of DU145CR xenograft tumors with 10 mg/kg of CBZ, 7.5 mg/kg/day 1/3 dose (4.1 mg/kg/day) of CLO, CBZ + 1/3 CLO, or no treatment (cont). H) Pathway analysis of phosphoproteome down-regulated by CLO in DU145CR. The dotted squares indicate suppressed genes related to OXT signaling by CLO. I) Schematic of OXT-signaling pathway. Blue inverted triangles indicate molecules suppressed by CLO in DU145CR cells. J) Abundance ratio of phosphorylation in each molecule induced by CLO in DU145 and DU145CR cells. The phosphorylation status of controls in DU145 and DU145CR cells was set to one. K) Abundance ratio of phosphorylation in each molecule induced by OXT, CLO, and a combination of OXT and CLO. L) Direct cell count of DU145 cells treated with various doses of OXT. M) Viability of DU145CR cells treated with various doses of OXT and CBZ.

than that of DU145 tumors (Fig. 3F). To test the synergistic effect of CBZ and CLO in vivo, we administered CLO in combination with CBZ. Consistent with the in vitro results, CBZ and CLO exerted a synergistic effect on DU145CR tumors (Fig. 3G). The mice that received CLO did not have any body weight loss, renal, hepatic, or pulmonary disorders (Fig. S13A and B). CLO also had a greater antitumor effect on PC3CR than on PC3 in vivo (Fig. S12C and D). These results suggest that CLO is a promising candidate for overcoming CBZ-resistant prostate cancer.

To explore the potential targets of CLO in prostate cancer, we performed a mass spectrometric phosphoproteome analysis. Pathway analysis showed that the OXT-signaling pathway was significantly inhibited by CLO (Fig. 3H and I) in DU145CR cells, whereas pimozide, which we have previously reported as another drug for overcoming CBZ resistance, did not inhibit OXT signaling; however, it inhibited other pathways, such as nucleocytoplasmic transport and 5′ adenosine monophosphate-activated protein kinase signaling pathways (Fig. S14).

Although phosphorylation of CAMK2D/G, EEE2K, GNAI2, MAPK1, PLCB3, PRKAA1, and ROCK2 was not inhibited in DU145 cells, their phosphorylation was down-regulated in DU145CR cells by CLO treatment (Fig. 3J). OXT administration up-regulated downstream signaling, whereas CLO inhibited it in DU145CR (Fig. 3K). We also investigated the effects of OXT on cell proliferation and CBZ resistance in prostate cancer. Whereas OXT did not promote cell proliferation (Fig. 3L), it reduced the CBZ sensitivity of DU145 cells (Fig. 3M).

We examined the effect of OXTR inhibition by treating DU145 and DU145CR cells with the OXTR inhibitor atosiban. Atosiban did not exert any antitumor effect until the concentration reached as high as 10 μM. There was no significant difference in the sensitivity to atosiban between DU145 and DU145CR cells (Fig. S15). The inhibitory effect of atosiban for phosphorylating OXTR signaling molecules was weaker than that of CLO, as evidenced by mass spectrometric phosphoproteome analysis results (Fig. S16).

Clinical significance of OXT signaling in patients with prostate cancer

To investigate the clinical significance of OXT-signaling molecules, we compared their expression in patients with primary prostate cancer ($n = 47$) and CBZ-resistant prostate cancer ($n = 10$) at our institute. OXTR and PLCB3 were significantly up-regulated in CBZ-resistant prostate cancer cases than in primary cases (Fig. 4A and B). OXTR and PLCB3 expressions were also higher in DU145CR xenograft tumors than in DU145 tumors, and it was suppressed by CLO administration (Fig. 4C and D).

To validate these results, we analyzed the correlation between prostate cancer prognosis and the expression of genes related to OXT signaling using The Cancer Genome Atlas (TCGA) prostate cancer cohort data (22). OXTR expression was not a significant predictor of prostate cancer outcome. Among the OXT-signaling-related genes, PLCB2 and PLCB3 were highly expressed in prostate cancer cases with a poorer prognosis, although the difference was not significant (Fig. S17A). The patient group with high expression of one or more of the PLCB family members (PLCB1-3) had a significantly poorer prognosis than the group with low expression (Fig. S17B).

We also analyzed the changes in OXT-signaling expression from primary prostate cancer into CRPC using publicly available microarray data (GSE35988 (23) and GSE3325 (24)). OXTR and PLCB3 expressions were higher in CRPC tissues than in primary prostate cancer (Fig. 4E).

Discussion

In this study, we performed single-cell RNA-seq of CTCs in patients with CBZ-resistant CRPC. Figure S18 summarizes OXT-related genes activated in CBZ-resistant prostate cancer identified via single-cell RNA-seq of CTCs, spatial gene expression analysis of prostate cancer tissues, and phosphorylation analysis of DU145CR cells. In our study of CBZ-resistant prostate cancer, we conducted an immunohistochemistry (IHC) analysis to assess the expression of OXTR and PLCB3. Our results indicated higher expression of these molecules in CBZ-resistant tumors compared to primary prostate cancer. We also conducted a survival analysis using TCGA cohort data and observed that elevated expression of downstream molecules in the OXT-signaling pathway was linked to poorer prognosis. It is important to note that the TCGA cohort primarily consists of early stage prostate cancer patients, which differs from CBZ-resistant cases. Therefore, it is vital to emphasize that there is currently no available NGS cohort that combines survival and mRNA expression data to definitively identify CBZ resistance development in patients. To address this limitation, it is crucial to consider conducting a prospective cohort study with a consistent patient population for future prognosis analyses. Additionally, our analysis of publicly available gene expression data revealed increased OXTR expression in CRPC compared to early stage prostate cancer. These findings, along with the TCGA data analysis, further underscore the clinical relevance of the OXT-signaling pathway.

We also identified the OXT-signaling pathway as a target of CLO. CLO is an oral antitussive drug that acts directly on the cough center of the nervous system and is used clinically to relieve coughing. Mechanistically, CLO inhibits histamine receptors (25) or 5-hydroxytryptamine receptors (26). However, there have been no reports on the anticancer properties of CLO in CRPC. We have previously reported that mitogen-activated protein kinase (MEK)/extracellular signal-regulated kinase (ERK) signaling is related to CBZ resistance and that a MEK inhibitor is effective for CBZ-resistant CRPC (13). However, no MEK/ERK inhibitors have been approved for the treatment of prostate cancer. Since the KEGG pathway analysis did not provide clear insights into the involvement of OXT and OXTR in the development of CBZ resistance, we conducted experiments involving the administration of OXT agonists/antagonists to prostate cancer model cell lines. These agents were administered to assess their impact on cell proliferation and CBZ sensitivity. While the administration of OXT agonists had no significant effect on cell proliferation, it did reduce CBZ sensitivity. This provides evidence that the factor contributing to CBZ resistance is likely associated with signal transduction through G proteins activated by OXTR. Additionally, in our analysis using publicly available gene expression data, we observed an up-regulation of OXTR expression in CRPC compared to early stage prostate cancer (Fig. 4E), suggesting that the signaling pathway is utilized in prostate cancer. Although the exact underlying mechanism requires further clarification in future studies, our findings indicate that CLO effectively suppressed the phosphorylation of OXT-signaling molecules specifically in CBZ-resistant prostate cancer. Furthermore, our established organoid, KOB023, derived from a patient who clinically developed resistance to CBZ treatment, displayed strong resistance to CBZ (Fig. S19). On the other hand, CLO inhibited the proliferation of KBO100 cells in a concentration-dependent manner (Fig. S19). These results collectively suggest that CLO holds promise as a potential candidate for combating CBZ resistance in prostate cancer. The research schema is depicted in Fig. 4F.

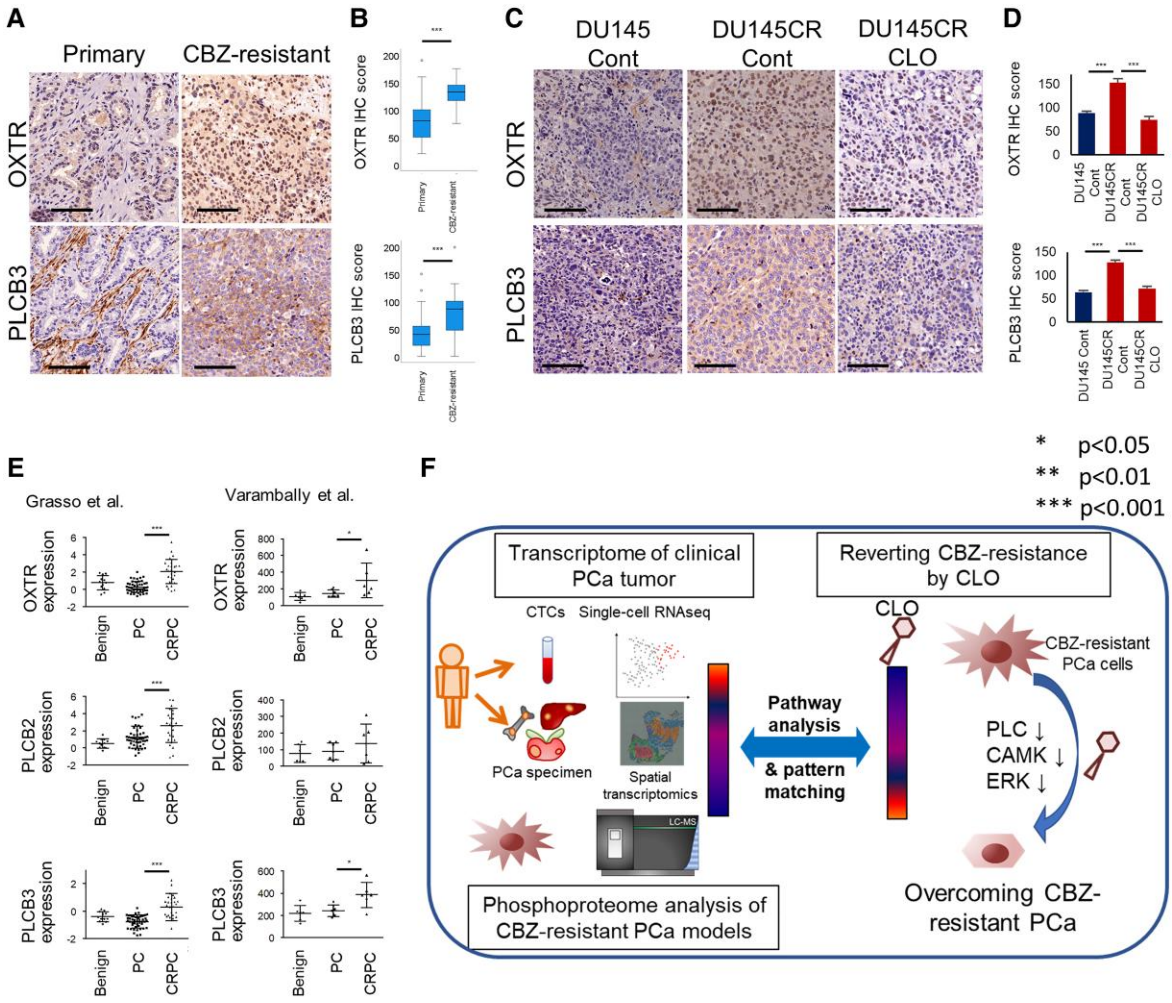

Fig. 4. Protein expression of OXT-signaling molecules was analyzed in patients with prostate cancer. A) Representative images of OXTR and PLCB3 IHC in primary and CBZ-resistant prostate cancer cases. The scale bars indicate 100 μm. B) Box–whisker plots showing the distribution of IHC scores for OXTR and PLCB3 in prostate cancer cases. C) Representative images of OXTR and PLCB3 IHC in DU145 and DU145CR xenograft tumors. Scale bars indicate 100 μm. D) The IHC score of OXTR and PLCB3 in xenograft tumors. E) High expression of OXT signaling is associated with CRPC development. Public microarray data (GSE35988 and GSE3325) were used for gene expression analysis. PC, localized prostate cancer; CRPC, metastatic CRPC. The Mann–Whitney *U* test was used to compare the mRNA expression levels between PC and CRPC. F) Schema of this study.

Current drug discovery processes, such as high-throughput screening, require a long time and abundant resources. Bioinformatic screening using drug databases is an economical primary screening tool. In our screening, we used the Connectivity Map (14), an online database of transcriptome changes induced by chemicals or genetic modifications. A Connectivity Map has been used in previous studies, reporting on novel candidate drugs that restore transcriptomic signatures of various diseases to the normal signature (27–31). We have previously described ribavirin, pimozide, and etoposide as potentially promising drugs for reverting genetic networks related to taxane resistance in CRPC, as evidenced by in silico screening using the Connectivity Map (15, 17, 18). We integrated pathway analysis of the drugs in the in silico screen with the single-cell RNA-seq data of CTCs of patients, revealing CLO as a drug targeting OXT signaling in CBZ-resistant CRPC.

CTCs are tumor cells that circulate in the blood of patients with cancer and may be used as liquid biopsies to screen for biomarkers and guide treatment selection. Although prostate cancer alters gene expression networks as it develops treatment resistance (4, 5, 32–38), serially biopsy recurrent or metastatic tumors in patients is often not possible. A liquid biopsy is particularly useful in such cases. However, there is no consensus on how to enrich and analyze CTCs, and it remains unclear whether a liquid biopsy is an alternative to a conventional solid biopsy. We have previously reported that the androgen receptor (AR) status of CTCs from patients with CRPC could be a potential biomarker for optimal treatment (7). Based on this established platform, we concentrated on CTCs and performed single-cell RNA-seq to explore therapeutic targets for CBZ-resistant prostate cancer. We found that CTCs in the four patients showed intrapatient heterogeneity in gene expression. This heterogeneity may underly a CBZ-resistance mechanism, and we identified OXT signaling as a CBZ-resistance factor from a heterogeneous population.

Although single-cell RNA-seq of CTCs was effective for investigating intrapatient heterogeneity, it cannot provide tumor location information. Therefore, spatial gene expression of prostatic tumor tissues was analyzed using the Visium platform. Consistent with the results of single-cell analysis in CTCs, spatial transcriptome confirmed heterogeneity in prostatic tumors. Our previous microarray analysis showed that gene clusters related to cell division and mitotic nuclear division were enhanced in the

CBZ-resistant cell line DU145CR, and activation of MEK/ERK signaling was observed as a mechanism of enhancement of these gene clusters; mRNA expression of OXT-signaling molecules was not enhanced in DU145CR (13). In this study, LC–MS results showed increased phosphorylation of OXT-signaling molecules in DU145CR, and CLO inhibited the phosphorylation of these molecules.

OXT functions as both a posterior pituitary hormone and a neurotransmitter involved in various biological processes, such as reproduction and social behavior. In relation to prostatic tissues, OXT reduced the suppressive effect of castration on normal prostate cell proliferation (39), and its antagonist has been tested in benign prostatic hyperplasia (40). Regarding prostate cancer, OXT induced the migration of prostate cancer cells in vitro (41), and the serum OXT levels were significantly higher in patients with prostate cancer than in healthy individuals (42). The OXT–OXTR axis promotes cancer through the MEK/ERK pathway or protein kinase C. OXTR was overexpressed in hepatocellular carcinoma (43), lung cancer (44), and breast cancer (45). There has been only limited published research related to the involvement of OXTR in prostate cancer (46, 47), and the relationship between OXTR signaling and treatment resistance in prostate cancer is still unclear. In our previous study, we demonstrated the involvement of the mitogen-activated protein kinase (MAPK) signal in the development of CBZ resistance (13). In this study, we observed that CLO had a suppressive effect on the MAPK signal. Furthermore, considering the documented cross-talk between the AR signal and the MAPK signal in prior studies (48–50), it is plausible to hypothesize that the OXT signal could potentially amplify the AR signal through the MAPK pathway.

PLCB, which was also up-regulated in CBZ-resistant prostate cancer tissue in this study, is an enzyme that triggers second messenger production in the inositol phospholipid metabolic system. G-protein-coupled receptors, such as OXTR, glutamate receptors, and muscarinic acetylcholine receptors activate PLCB. PLCB expression is a poor prognostic factor in several cancers (51). Although PLCB3 promoted prostate cancer progression (52) in vitro, no reports have shown its involvement in treatment resistance in prostate cancer.

In this study, OXT-signaling molecules, including OXTR and PLCB3, were up-regulated in CBZ-resistant prostate cancer. OXTR and PLCB3 expressions were especially higher in AR-signaling positive, neuroendocrine prostate cancer-marker-negative tumors. Prostatic OXT concentrations were regulated by androgen, and a 5α-reductase inhibitor, finasteride, increased prostatic OXT levels (53). Although the detailed mechanisms remain unclear, tumor microenvironment under androgen-deprived conditions may be related to enhanced OXT signaling. CLO had a stronger inhibitory effect on OXT signaling in CBZ-resistant cancer than in CBZ-sensitive cancers. In addition, CLO had stronger antitumor activity than the OXTR inhibitor atosiban. Because CLO has many off-target effects, its OXTR inhibitory activity may be an indirect effect mediated by an unknown mechanism. We confirmed heterogeneity in CBZ-resistant prostate cancer, and CLO seemed effective for some specific prostate cancer populations. For the clinical application of CLO, it is necessary to search for biomarkers of therapeutic response, and our results suggest that OXTR and PLCB3 expression could be biomarkers for CLO. It is also necessary to study the possibility of administering CLO in combination with other drugs, including CBZ.

In conclusion, we identified the OXT-signaling pathway as a potential target for CBZ-resistant CRPC using single-cell transcriptomic analysis of CTCs. CLO may potentially overcome CBZ resistance in CRPC by inhibiting the OXT-signaling pathway.

Materials and methods

Animals

Animal experiments were conducted following previously described protocols (17, 18). Five- to seven-week-old male athymic nude BALB/c mice were used for murine experiments. The animal experiments were approved by the Keio University Institutional Animal Committee (approval number: 16036), and animal care was performed in accordance with Keio University guidelines for animal experiments.

Cell lines

Human prostate cancer cell lines were cultured according to established protocols (17, 18). CRPC cell lines DU145 and PC3 were obtained from the American Type Culture Collection. DU145CR cells were established by incubating DU145 cells with gradually increasing concentrations of CBZ (13). DU145 and DU145CR cells were routinely maintained in Roswell Park Memorial Institute-1640 (Invitrogen, Carlsbad, CA, USA) supplemented with 10% fetal bovine serum (Dainippon Pharmaceutical, Tokyo, Japan) at 37 °C in a humidified 5% CO_2 atmosphere.

Human subjects

Surgical specimens from patients who underwent radical prostatectomy for primacy prostate cancer ($n = 47$) and transurethral resection of the prostate for CBZ-resistant prostate cancer ($n = 10$), collected at Keio University Hospital, were retrospectively analyzed in this study. This study was approved by the Keio University School of Medicine Ethics Committee (approval numbers: 20140159 and 20150285).

Single-cell sequencing of CTCs

Circulating tumor cell (CTC) concentration and single-cell RNA-seq were conducted following previously established protocols (7, 18). We collected and concentrated CTCs from patients with metastatic CRPC who developed acquired CBZ resistance following CBZ chemotherapy, using the ClearCell FX System (Biolidics Ltd, Mapex, Singapore), an automated CTC enrichment system powered by a microfluidic biochip. To count the CTCs isolated using this system, immunostaining was performed using the following antibodies: mouse antipan human keratin (C11) monoclonal antibody (mAb; keratin 4, 5, 6, 8, 10, 13, and 18; Cell Signaling, Danvers, MA, USA), mouse antihuman cytokeratin mAb (CK3-6H5; Miltenyi Biotec, Bergisch Gladbach, Germany), mouse antihuman EpCAM (VU1D9) mAb (Cell Signaling, Danvers, MA, USA), and rabbit CD45 (D9M81) mAb (Cell Signaling). We defined CTCs as cells with keratin, cytokeratin, or EpCAM expression but without CD45 expression. Single-cell RNA-seq of label-free CTCs was performed using the ***10× Genomics platform (10× Genomics, Pleasanton, CA, USA). Illumina cDNA libraries of PC3 and PC3CR cells were generated using the Chromium Single Cell 3 Chip Kit V2 (10× Genomics). Illumina libraries were sequenced on an Illumina HiSeq4000 with reads 1 = 26 bp and 2 = 134 bp. The reads underwent demultiplexing and collapsing, starting with the initial identification of the 1,500 cellular barcodes. These barcodes were then perfectly matched with the most frequent cell barcodes, followed by filtering to retain only the unique combinations of cell barcodes and 10× unique molecular identifiers. The raw data were processed using Cell Ranger 2.2.0 (10× Genomics) to generate a gene–cell expression matrix.

Spatial gene expression analysis

The spatial gene expression of tumor tissue was analyzed using the 10× Genomics Visium platform (54). Frozen prostate cancer TUR (transurethral-resection) specimens were preserved in an optimal cutting temperature compound (Sakura Finetek, Tokyo, Japan). Thinly sliced tissue was placed on Visium spatial gene expression slides (10× Genomics). The sliced tissues were processed, and library preparation for RNA sequencing was performed according to the manufacturer's instructions. Illumina libraries were sequenced on an Illumina HiSeq4000. FASTQ files obtained from HiSeq4000 were processed using Space Ranger software version 1.0.0 (10× Genomics). The processed spatial gene expression data were analyzed using the Loupe Browser version 6.0 (10× Genomics).

Water-soluble tetrazolium cell viability assay

Water-soluble tetrazolium (WST) cell viability assay was performed as previously reported (17, 18). DU145 and DU145CR cells were seeded in 96-well plates, allowed to attach for 24 h, and treated with varying concentrations of CBZ (WAKO, Tokyo, Japan) and CLO (Sigma-Aldrich, St Louis, MO, USA) for 48 h. At the end of the 48 h incubation period, WST reagents were added to each well, and the cells were incubated for 1 h. Cell viability was estimated by colorimetry in an iMark plate reader (Bio-Rad Laboratories, Hercules, CA, USA) at 570 nm.

Murine xenograft prostate cancer model

We evaluated the in vivo efficacy of CLO for CBZ-resistant prostate cancer xenograft mice model as previously reported (17, 18). Five- to seven-week-old male athymic nude BALB/c mice were castrated by a scrotal incision under anesthesia to create a xenograft model. PC3 and PC3CR cells (2×10^6 cells) suspended in 100 μL Matrigel (Becton Dickinson Labware, Lincoln Park, NJ, USA) were subcutaneously inoculated into mice. Tumors were measured every 4 days. When the mean tumor volume reached ~100 mm^3, the mice were randomly assigned to one of four groups, with eight mice per group: an untreated control group or three treatment groups treated with intraperitoneal CBZ only (10 mg/kg), peroral CLO only (12.5 or 4.1 mg/kg/day), or intraperitoneal CBZ (10 mg/kg) combined with peroral CLO (4.1 mg/kg/day). The initial dosage of CLO administered to mice was set at a maximum of 12.5 mg/kg/day, considering previous literature where a maximum dose of 30 mg/kg/day was employed without significant adverse effects (26, 55). On day 17, the mice were anesthetized with sevoflurane (WAKO) and euthanized by cervical dislocation. Subcutaneous tumors were harvested.

Mass spectrometric phosphoproteome analysis

We performed mass spectrometric analysis according to previously established protocols (56, 57). The cell pellets were lysed in (20 mM 4-(2-hydroxyethyl)-1-piperazineethanesulfonic acid (HEPES)–NaOH [pH 8.0], 12 mM sodium deoxycholate, and 12 mM sodium *N*-lauroylsarcosinate). After reduction with 10 mM Tris(2-carboxyethyl)phosphine at 37 °C for 30 min, alkylation with 50 mM iodoacetamide at ambient temperature for 45 min, and five times dilution with (20 mM HEPES–NaOH [pH = 8.0]), 100 μg of protein was digested with trypsin/Lys-C mix (Promega) at 37 °C for 12 h. After removing sodium deoxycholate and sodium *N*-lauroylsarcosinate by ethyl acetate extraction, the resulting peptides were desalted using a C18 cartridge (3M, Maplewood, MN, USA). Subsequently, phosphopeptides were purified using a high-select TiO_2 phosphopeptide enrichment kit (Thermo Fisher Scientific, Waltham, MA, USA) according to the manufacturer's instructions. The resulting peptides were analyzed using an Orbitrap Fusion Lumos mass spectrometer (Thermo Fisher Scientific) combined with UltiMate 3000 rapid separation liquid chromatography nano-flow high-performance liquid chromatography (Thermo Fisher Scientific). Peptides were enriched with μ-Precolumn (0.3 mm id × 250 mm, 1.6 μm; Ion Opticks Pty Ltd, Australia) using the two-step gradient; 2–40% acetonitrile for 110 min, followed by 40–95% acetonitrile for 5 min in the presence of 0.1% formic acid. The analytical parameters of Orbitrap Fusion Lumos were set as follows: the resolution of full scans = 50,000, scan range (m/z) = 350–1,500, maximum injection time of full scans = 50 ms, automatic gain control (AGC) target of full scans = 4×10^5, dynamic exclusion duration = 30 s, the cycle time of data-dependent MS/MS acquisition = 2 s, activation type = higher energy collisional dissociation, the MS/MS detector = ion trap, maximum injection time of MS/MS = 35 ms, and AGC target of MS/MS = 1×10^4. The MS/MS spectra were searched against the *Homo sapiens* protein sequence database in SwissProt using Proteome Discoverer 2.4 software (Thermo Fisher Scientific), in which peptide identification filters were set at a false discovery rate of <1%. Label-free relative quantification analysis was performed with the default parameters of the Minora feature detector node, feature mapper node, and precursor ions quantifier node in proteome Discoverer 2.4 software.

Microarray gene expression analysis

We performed microarray according to previously established protocols (17, 18). Total RNA was isolated from DU145, DU145CR, PC3, and PC3CR cells using an RNeasy Mini Kit (Qiagen, Valencia, CA, USA). Gene expression profiles were determined using the Affymetrix GeneChip Human Gene 1.0 ST array, according to the manufacturer's instructions. After generating single-stranded cDNA, fragmentation and sense-strand cDNA labeling were performed using an Affymetrix GeneChip WT terminal labeling kit (Affymetrix, Santa Clara, CA, USA) according to the manufacturer's protocol. After hybridization, GeneChip Fluidics Station 450 (Affymetrix) was used to wash the arrays. Scanning was performed using GeneChip Scanner 3000 7G (Affymetrix). The raw intensity data from the scanned images of the microarrays were preprocessed using Affymetrix Expression Console software 1.4.1. Expression intensities were stored as cell intensity (CEL) files, and the CEL files were normalized using the robust multichip average method. To identify compounds that could reprogram the CBZ-resistance-related genetic network, the CBZ resistance signature was established by calculating the 2-fold gene changes from DU145 to DU145CR, after which the probe list of the CBZ resistance signature was entered into the connectivity map (http://www.broadinstitute.org/cmap/). According to the connectivity map system (14, 15, 27–31, 58), the top 500 up- and down-regulated probes, compatible with the HG-U133A platform, were used. The significance threshold for the candidate compounds was set at $P < 0.05$.

Pathway analysis

The biological function of each gene was analyzed using the DAVID tool (https://david.ncifcrf.gov/). We entered gene lists up- or down-regulated by the biological states of drug administration into the DAVID functional annotation clustering tool (https://david.ncifcrf.gov/) and explored the pathways enriched by the listed genes.

Immunohistochemistry

Immunohistochemical staining was performed as previously reported (17, 18). Mice xenograft tumors and surgical specimens from patients were used for this study. We immunostained 4-μm-thick sections of formalin-fixed, paraffin-embedded xenograft tumors. Endogenous peroxidase activity was blocked with 1% hydrogen peroxide after antigen retrieval using citric acid (pH 6.0). The samples were treated with polyclonal anti-OXTR antibodies (Invitrogen, Thermo Fisher Scientific, Waltham, MA, USA) diluted at 1:50 and anti-PLCB3 mAb (Santa Cruz Biotechnology, Santa Cruz, CA, USA) diluted at 1:400, and then with secondary antibodies conjugated to peroxidase-labeled dextran polymer. The immunoreaction was visualized using diaminobenzidine and counterstained with 10% hematoxylin. The histoscores for OXTR and PLCB3 were calculated based on the mean percentage intensity (range: 0–300).

Quantification and statistical analysis

Data analysis of prostate cancer cohorts and experiments was conducted following previously reported methods (17, 18). Recurrence-free survival and mRNA expression in the TCGA prostate cancer dataset (22) were extracted from the cBioPortal (http://www.cbioportal.org/). The prognostic significance of the expression of each gene was examined using Kaplan–Meier survival analysis, and recurrence-free survival outcomes were compared using log-rank tests.

The experiments were repeated at least three times. Statistical analysis was performed using the *t*-test and Tukey–Kramer method for multiple comparison tests. Statistical significance was set at $P < 0.05$.

Acknowledgments

The authors thank Yoko Suzuki and Natsumi Aoki for their technical assistance.

Supplementary Material

Supplementary material is available at *PNAS Nexus* online.

Funding

This study was supported by the grants-in-aid for Scientific Research (grant numbers 21K09436 and 20K22822 to H.H. and 21K1957 and 20H03817 to T.K.) from the Ministry of Education, Culture, Sports, Science and Technology; the Keio University Grant-in-Aid for Encouragement of Young Medical Scientists (grant numbers 02-002-0014 and 02-002-0020 to H.H.) from School of Medicine Keio University; The Japanese Foundation for Prostate Research, Japan; a research grant to T.K. from the Japanese Urological Association; Japan Agency for Medical Research and Development (grant number A295TS to H.H. and grant number A399TS to T.K.) from Japan Agency for Medical Research and Development; Keio Gijuku Fukuzawa Memorial Fund for the Advancement of Education and Research; and SGH Foundation.

Author Contributions

Conceptualization: H.H. and T.K.; methodology: H.H. and T.K.; acquisition of tumor specimens and clinical data: Y.B. and Y.Y.; investigation: H.H., T.K., K.I.T., K.U., Y.S., S.I., and H.B.; evaluation: M.O.; project administration: H.H. and T.K.; writing—original draft: H.H., T.K., K.I.T., S.I., and H.B.; writing—review and editing: Y.B., Y.Y., K.U., Y.S., and M.O.

Data Availability

The microarray data pertaining to prostate cancer cell lines (GSE110107 and GSE182619) can be accessed through the gene expression omnibus (GEO) database, available at https://www.ncbi.nlm.nih.gov/geo/. In addition, the public microarray data (GSE35988 and GSE3325) employed in our analysis are also obtainable from the GEO repository. Furthermore, the recurrence-free survival and mRNA expression data from the TCGA prostate cancer dataset (22) were extracted from the cBioPortal, which can be accessed at http://www.cbioportal.org/.

References

1 Rawla P. 2019. Epidemiology of prostate cancer. *World J Oncol*. 10(2):63–89.
2 Kosaka T, Shinojima T, Morita S, Oya M. 2018. Prognostic significance of grade 3/4 neutropenia in Japanese prostate cancer patients treated with cabazitaxel. *Cancer Sci*. 109(5):1570–1575.
3 Kosaka T, Hongo H, Mizuno R, Oya M. 2018. Risk stratification of castration-resistant prostate cancer patients treated with cabazitaxel. *Mol Clin Oncol*. 9(6):683–688.
4 Hongo H, Kosaka T, Nakatsuka S, Oya M. 2021. A long-term survivor of metastatic neuroendocrine prostate cancer treated with multimodal therapy: genetic consideration from next-generation sequencing. *Int Cancer Conf J*. 10(3):174–180.
5 Hongo H, Kosaka T, Aimono E, Nishihara H, Oya M. 2020. Aggressive prostate cancer with somatic loss of the homologous recombination repair gene FANCA: a case report. *Diagn Pathol*. 15(1):5.
6 Hongo H, *et al*. 2022. A first Japanese case of intraductal cancer of the prostate with checkpoint kinase 2 mutation. *Asian J Urol*. 9(4):480–482.
7 Kosaka T, Hongo H, Oya M. 2019. Complete response with early introduction of cabazitaxel in a patient with multiple lung metastases of castration-resistant prostate cancer following the early detection of metastases using liquid biopsy: a case report. *BMC Cancer*. 19(1):562.
8 Conteduca V, *et al*. 2021. Circulating tumor cell heterogeneity in neuroendocrine prostate cancer by single cell copy number analysis. *NPJ Precis Oncol*. 5(1):76.
9 Sun Y-F, *et al*. 2021. Dissecting spatial heterogeneity and the immune-evasion mechanism of CTCs by single-cell RNA-seq in hepatocellular carcinoma. *Nat Commun*. 12(1):4091.
10 Cheng YH, *et al*. 2019. Hydro-seq enables contamination-free high-throughput single-cell RNA-sequencing for circulating tumor cells. *Nat Commun*. 10(1):2163.
11 Situ B, *et al*. 2020. Identification and single-cell analysis of viable circulating tumor cells by a mitochondrion-specific AIE bioprobe. *Adv Sci (Weinh)*. 7(4):1902760.
12 Cann GM, *et al*. 2012. mRNA-seq of single prostate cancer circulating tumor cells reveals recapitulation of gene expression and pathways found in prostate cancer. *PLoS One*. 7(11):e49144.
13 Hongo H, Kosaka T, Oya M. 2018. Analysis of cabazitaxel-resistant mechanism in human castration-resistant prostate cancer. *Cancer Sci*. 109(9):2937–2945.
14 Lamb J, *et al*. 2006. The Connectivity Map: using gene-expression signatures to connect small molecules, genes, and disease. *Science*. 313(5795):1929–1935.

15 Kosaka T, *et al.* 2013. Identification of drug candidate against prostate cancer from the aspect of somatic cell reprogramming. *Cancer Sci*. 104(8):1017–1026.

16 Takayama KI, *et al.* 2021. Subtype-specific collaborative transcription factor networks are promoted by OCT4 in the progression of prostate cancer. *Nat Commun*. 12(1):3766.

17 Hongo H, Kosaka T, Suzuki Y, Oya M. 2021. Discovery of a new candidate drug to overcome cabazitaxel-resistant gene signature in castration-resistant prostate cancer by in silico screening. *Prostate Cancer Prostatic Dis*. 26(1):59–66.

18 Hongo H, *et al.* 2021. Topoisomerase II alpha inhibition can overcome taxane-resistant prostate cancer through DNA repair pathways. *Sci Rep*. 11(1):22284.

19 Wang S, *et al.* 2021. Molecular imaging of prostate cancer targeting CD46 using ImmunoPET. *Clin Cancer Res*. 27(5):1305–1315.

20 Su Y, *et al.* 2018. Targeting CD46 for both adenocarcinoma and neuroendocrine prostate cancer. *JCI Insight*. 3(17):e121497.

21 Ghandi M, *et al.* 2019. Next-generation characterization of the Cancer Cell Line Encyclopedia. *Nature*. 569(7757):503–508.

22 Cancer Genome Atlas Research Network. 2015. The molecular taxonomy of primary prostate cancer. *Cell*. 163(4):1011–1025.

23 Grasso CS, *et al.* 2012. The mutational landscape of lethal castration-resistant prostate cancer. *Nature*. 487(7406):239–243.

24 Varambally S, *et al.* 2005. Integrative genomic and proteomic analysis of prostate cancer reveals signatures of metastatic progression. *Cancer Cell*. 8(5):393–406.

25 Daddam JR, Sreenivasulu B, Peddanna K, Umamahesh K. 2020. Designing, docking and molecular dynamics simulation studies of novel cloperastine analogues as anti-allergic agents: homology modeling and active site prediction for the human histamine H1 receptor. *RSC Adv*. 10(8):4745–4754.

26 Soeda F, Hirakawa E, Inoue M, Shirasaki T, Takahama K. 2014. Cloperastine rescues impairment of passive avoidance response in mice prenatally exposed to diethylstilbestrol. *Environ Toxicol*. 29(2):216–225.

27 Wei G, *et al.* 2006. Gene expression-based chemical genomics identifies rapamycin as a modulator of MCL1 and glucocorticoid resistance. *Cancer Cell*. 10(4):331–342.

28 De Preter K, *et al.* 2009. Meta-mining of neuroblastoma and neuroblast gene expression profiles reveals candidate therapeutic compounds. *Clin Cancer Res*. 15(11):3690–3696.

29 Iorio F, *et al.* 2010. Discovery of drug mode of action and drug repositioning from transcriptional responses. *Proc Natl Acad Sci U S A*. 107(33):14621–14626.

30 Barabasi AL, Gulbahce N, Loscalzo J. 2011. Network medicine: a network-based approach to human disease. *Nat Rev Genet*. 12(1):56–68.

31 Kunkel SD, *et al.* 2011. mRNA expression signatures of human skeletal muscle atrophy identify a natural compound that increases muscle mass. *Cell Metab*. 13(6):627–638.

32 Best CJ, *et al.* 2005. Molecular alterations in primary prostate cancer after androgen ablation therapy. *Clin Cancer Res*. 11(19 Pt 1): 6823–6834.

33 Baba Y, *et al.* 2022. Castration-resistant prostate cancer patient presenting with whole genome doubling with CDK-12 mutation. *BMC Med Genomics*. 15(1):32.

34 Umeda K, *et al.* 2020. A Japanese patient with ductal carcinoma of the prostate carrying an adenomatosis polyposis coli gene mutation: a case report. *Diagn Pathol*. 15(1):102.

35 Daimon T, *et al.* 2021. Prominent response to platinum-based chemotherapy in a patient with BRCA2 mutant-neuroendocrine prostate cancer and MDM2 amplification. *IJU Case Rep*. 4(4): 216–219.

36 Shojo K, *et al.* 2021. First case of ductal adenocarcinoma of the prostate with MAP3K1 homozygous deletion. *IJU Case Rep*. 4(3): 176–179.

37 Watanabe K, *et al.* 2019. Japanese case of enzalutamide-resistant prostate cancer harboring a SPOP mutation with scattered allelic imbalance: response to platinum-based therapy. *Clin Genitourin Cancer*. 17(5):e897–e902.

38 Kobayashi H, *et al.* 2021. A first case of ductal adenocarcinoma of the prostate having characteristics of neuroendocrine phenotype with PTEN, RB1 and TP53 alterations. *BMC Med Genomics*. 14(1):245.

39 Piećaš B, Popović A, Jovović D, Hristić M. 1992. Mitotic activity and cell deletion in ventral prostate epithelium of intact and castrated oxytocin-treated rats. *J Endocrinol Invest*. 15(4): 249–253.

40 Lee SN, *et al.* 2021. Oxytocin receptor antagonists as a novel pharmacological agent for reducing smooth muscle tone in the human prostate. *Sci Rep*. 11(1):6352.

41 Zhong M, Boseman ML, Millena AC, Khan SA. 2010. Oxytocin induces the migration of prostate cancer cells: involvement of the Gi-coupled signaling pathway. *Mol Cancer Res*. 8(8): 1164–1172.

42 Xu H, *et al.* 2017. The function of oxytocin: a potential biomarker for prostate cancer diagnosis and promoter of prostate cancer. *Oncotarget*. 8(19):31215–31226.

43 Hu B, Yang XB, Sang XT. 2021. Molecular subtypes based on immune-related genes predict the prognosis for hepatocellular carcinoma patients. *Int Immunopharmacol*. 90:107164.

44 Péqueux C, Breton C, Hagelstein MT, Geenen V, Legros JJ. 2005. Oxytocin receptor pattern of expression in primary lung cancer and in normal human lung. *Lung Cancer*. 50(2):177–188.

45 Ito I, *et al.* 1995. Expression of the oxytocin receptor in clinical human breast cancer tissues. *Adv Exp Med Biol*. 395:555–556.

46 Cassoni P, Marrocco T, Sapino A, Allia E, Bussolati G. 2004. Evidence of oxytocin/oxytocin receptor interplay in human prostate gland and carcinomas. *Int J Oncol*. 25(4):899–904.

47 Zhong M, Clarke S, Vo BT, Khan SA. 2012. The essential role of Giα2 in prostate cancer cell migration. *Mol Cancer Res*. 10(10): 1380–1388.

48 Migliaccio A, *et al.* 2000. Steroid-induced androgen receptor-oestradiol receptor beta-Src complex triggers prostate cancer cell proliferation. *EMBO J*. 19(20):5406–5417.

49 Heinlein CA, Chang C. 2002. The roles of androgen receptors and androgen-binding proteins in nongenomic androgen actions. *Mol Endocrinol*. 16(10):2181–2187.

50 Carey AM, *et al.* 2007. Ras-MEK-ERK signaling cascade regulates androgen receptor element-inducible gene transcription and DNA synthesis in prostate cancer cells. *Int J Cancer*. 121(3): 520–527.

51 Zhang T, *et al.* 2019. Distinct prognostic values of phospholipase C beta family members for non-small cell lung carcinoma. *Biomed Res Int*. 2019:4256524.

52 Shen D, Cao X. 2015. Potential role of CXCR3 in proliferation and invasion of prostate cancer cells. *Int J Clin Exp Pathol*. 8(7): 8091–8098.

53 Jenkin L, Nicholson HD. 1999. Evidence for the regulation of prostatic oxytocin by gonadal steroids in the rat. *J Androl*. 20(1):80–87.

54 Maynard KR, *et al.* 2021. Transcriptome-scale spatial gene expression in the human dorsolateral prefrontal cortex. *Nat Neurosci*. 24(3):425–436.

55 Johnson CM, Cui N, Xing H, Wu Y, Jiang C. 2020. The antitussive cloperastine improves breathing abnormalities in a Rett

syndrome mouse model by blocking presynaptic GIRK channels and enhancing GABA release. *Neuropharmacology*. 176:108214.
56 Saito Y, *et al.* 2022. Polarity protein SCRIB interacts with SLC3A2 to regulate proliferation and tamoxifen resistance in ER+ breast cancer. *Commun Biol*. 5(1):403.
57 Miyagi T, *et al.* 2023. Differential toxicity and localization of arginine-rich C9ORF72 dipeptide repeat proteins depend on declustering of positive charges. i*Science*. 26(6):106957.
58 Lamb J. 2007. The Connectivity Map: a new tool for biomedical research. *Nat Rev Cancer*. 7(1):54–60.